UNIVERSITY *of* York

This is a repository copy of *β-delayed fission and α decay of At196*.

White Rose Research Online URL for this paper:
https://eprints.whiterose.ac.uk/104870/

Version: Published Version

Article:

Truesdale, V. L., Andreyev, A. N. orcid.org/0000-0003-2828-0262, Ghys, L. et al. (35 more authors) (2016) β-delayed fission and α decay of At196. Physical Review C. 034308. pp. 1-11. ISSN 2469-9993

https://doi.org/10.1103/PhysRevC.94.034308

White Rose
university consortium
Universities of Leeds, Sheffield & York

eprints@whiterose.ac.uk
https://eprints.whiterose.ac.uk/

β-delayed fission and α decay of ^{196}At

V. L. Truesdale,[1] A. N. Andreyev,[1,2,3,*] L. Ghys,[4,5] M. Huyse,[4] P. Van Duppen,[4] S. Sels,[4] B. Andel,[6] S. Antalic,[6] A. Barzakh,[7]
L. Capponi,[3] T. E. Cocolios,[8,9] X. Derkx,[3,10] H. De Witte,[4] J. Elseviers,[4] D. V. Fedorov,[7] V. N. Fedosseev,[11]
F. P. Heßberger,[12,13] Z. Kalaninová,[6,14] U. Köster,[15] J. F. W. Lane,[3] V. Liberati,[3] K. M. Lynch,[9,16] B. A. Marsh,[11] S. Mitsuoka,[2]
Y. Nagame,[2] K. Nishio,[2] S. Ota,[2] D. Pauwels,[5] L. Popescu,[5] D. Radulov,[4] E. Rapisarda,[16] S. Rothe,[11,17] K. Sandhu,[3]
M. D. Seliverstov,[4,1,3,7] A. M. Sjödin,[11] C. Van Beveren,[4] P. Van den Bergh,[4] and Y. Wakabayashi[2]

[1]*Department of Physics, University of York, York Y010 5DD, United Kingdom*
[2]*Advanced Science Research Center, Japan Atomic Energy Agency, Tokai-Mura, Naka-gun, Ibaraki 319-1195, Japan*
[3]*School of Engineering, University of the West of Scotland, Paisley PA1 2BE, United Kingdom*
[4]*KU Leuven, Instituut voor Kern-en Stralingsfysica, 3001 Leuven, Belgium*
[5]*Belgian Nuclear Research Center SCK·CEN, Boeretang 200, B-2400 Mol, Belgium*
[6]*Department of Nuclear Physics and Biophysics, Comenius University, 84248 Bratislava, Slovakia*
[7]*Petersburg Nuclear Physics Institute, NRC Kurchatov Institute, Gatchina 188300, Russia*
[8]*PH Departement, CERN, CH-1211 Geneve 23, Switzerland*
[9]*School of Physics and Astronomy, The University of Manchester, Manchester M13 9PL, United Kingdom*
[10]*LPC, ENSICAEN, Université de Caen Basse Normandie, CNRS/IN2P3-ENSI, Caen F-14050, France*
[11]*EN Department, CERN, CH-1211 Geneve 23, Switzerland*
[12]*Gesellschaft für Schwerionenforschung, Planckstrasse 1, D-64291 Darmstadt, Germany*
[13]*Helmholtz Institut Mainz, 55099 Mainz, Germany*
[14]*Laboratory of Nuclear Problems, JINR, 141980 Dubna, Russia*
[15]*Institut Laue Langevin, 71 avenue des Martyrs, F-38042 Grenoble Cedex 9, France*
[16]*PH Department, CERN, CH-1211 Geneve 23, Switzerland*
[17]*Institut für Physik, Johannes Gutenberg-Universität Mainz, D-55128 Mainz, Germany*

A nuclear-decay spectroscopy study of the neutron-deficient isotope ^{196}At is reported where an isotopically pure beam was produced using the selective Resonance Ionization Laser Ion Source and On-Line Isotope Mass Separator (CERN). The fine-structure α decay of ^{196}At allowed the low-energy excited states in the daughter nucleus ^{192}Bi to be investigated. A β-delayed fission study of ^{196}At was also performed. A mixture of symmetric and asymmetric fission-fragment mass distributions of the daughter isotope ^{196}Po (populated by β decay of ^{196}At) was deduced based on the measured fission-fragment energies. A βDF probability $P_{\beta DF}(^{196}\text{At}) = 9(1) \times 10^{-5}$ was determined.

I. INTRODUCTION

The region of very neutron-deficient astatine isotopes provides a rich variety of interesting nuclear structure and decay phenomena. Shape coexistence at low excitation energy [1] and expected (yet unobserved) occurrence of proton emission in the lightest astatine isotopes are just two such examples. Over the past two decades, extensive nuclear-decay investigations have been performed for a long chain of the lightest astatine isotopes, both by particle decay (see, e.g., Refs. [2–5]) and by γ-ray spectroscopy (see, e.g., [6–9]).

One of the most important conclusions from the previous studies was the evidence for an onset of deformation at low excitation energy, demonstrated, e.g., by the behavior of excited states in $^{197-201}$At [6–9]. This is also corroborated by, e.g., the fact that, based on the α-decay systematics, the ground states of ^{191,193}At were interpreted as an intruder $1/2^+$ configuration [2], while the $1h_{9/2}$ proton is responsible for the ground state of all heavier odd-A astatine isotopes. β-delayed fission (βDF) is another interesting, albeit rare, phenomenon in this region, which recently attracted a lot of experimental and theoretical interest; see the recent review in Ref. [10] and references therein.

This paper reports on a detailed α-decay and βDF study of the neutron-deficient isotope ^{196}At. This work extends our recent α-decay spectroscopy and βDF investigations of ^{192}At [4,11] and ^{194}At [5,11,12].

β-delayed fission in the neutron-deficient nuclei is a two-step process in which a parent nucleus (A,Z) first undergoes β^+/EC decay, populating excited states in the daughter (A,Z-1) nuclide. If these states lie close to or above the fission barrier (B_f) of the daughter nucleus, there is a probability that the daughter nucleus will fission, in a competition with γ decay; see Refs. [10,13] and references therein. In βDF, the excitation energy of the daughter nucleus is limited by the Q_{EC} of the precursor ($E^* \leqslant Q_{EC}$). Usually, Q_{EC} does not exceed 9–12 MeV in the most neutron-deficient isotopes in
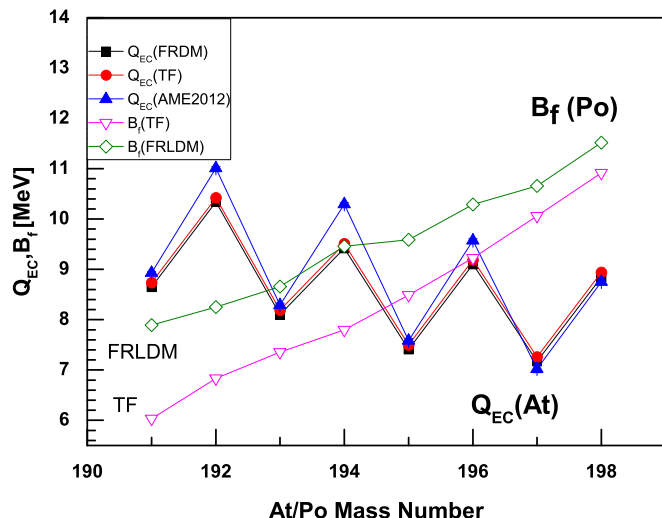
FIG. 1. Calculated Q_{EC}(At) (solid circle and square symbols) and B_f(Po) (open symbols) values from the FRDM/FRLDM [14,15] and from the TF model [16]. The Q_{EC} values from AME2012 [17] are shown by the solid triangles.

TABLE I. A comparison of α-decay energies E_α, half-life values $T_{1/2}$, relative intensities I_α, and deduced reduced α-decay widths δ_α^2 (where reported) for ^{196}At from our measurements and previous results. Our measured half-life value for ^{196}At is $T_{1/2} = 371(5)$ ms (see Sec. III B).

E_α (keV)	$T_{1/2}$ (ms)	I_α (%)	$Q_{\alpha,\mathrm{tot}}$ (keV)	δ_α^2 (keV)	Reference
7055(7)	300(100)				[18]
7053(30)	320^{+220}_{-90}				[29]
7044(7)	390^{+270}_{-120}				[30]
7065(30)	253(9)				[31]
7048(5)	388(7)				[32]
7055(12)	389(54)				[33]
7047(5)	350^{+50}_{-40}				[34]
7048(12)	350^{+290}_{-110}			27(2)	[35]
7045(5)	350(90)	96(2)		29(8)	[19]
6732(8)		4(2)		17(9)	[19]
7053(5)	371(5)	97.8(1)	7200(5)	26(1)	This work
6854(6)	365(167)	0.26(3)	7196(6)[b]	0.4(1)[a]	This work
6746(5)	343(45)	1.80(6)	7202(5)[b]	6.1(3)[a]	This work
6644(8)	413(637)	0.14(3)		1.2(3)[a]	This work

[a]Reduced widths were calculated by using the deduced half-life of 371(5) ms.
[b]The f.s. $Q_{\alpha,\mathrm{tot}}$ values were calculated using the α-γ coincidences of 6854-200 and 6746-316 keV.

the lead region, where βDF is possible [10]. βDF is therefore an important tool for studying low-energy fission ($E^* \sim B_f$) of exotic nuclei that do not decay by spontaneous fission from their ground state. An interesting application of βDF is the possibility to estimate the fission-barrier heights of daughter nuclei; see Ref. [13] and references therein.

Specifically for the astatine isotopes of our interest, the plot of Q_{EC}(At) and B_f(Po) values is given in Fig. 1. We note that neither the fission-barrier heights for the daughter polonium isotopes nor the experimental masses (thus Q_{EC} values) for some of these astatine isotopes are yet known. Therefore, for the consistency of the discussion (see also Ref. [10]) we prefer to use the calculated values, based on the finite range droplet model/finite range liquid drop model (FRDM/FRLDM) framework [14,15]. For comparison, the calculated values from the Thomas-Fermi (TF) model [16] and experimental (where known) or extrapolated Q_{EC} values from AME2012 [17] are also shown. One notices that while the calculated Q_{EC} values from both models agree quite well, the respective estimates of the fission-barrier heights differ by more than 1 MeV, with the TF values being consistently lower in comparison with the FRDM/FRLDM model. As an example, for βDF of ^{192}At, a rather large and positive energy difference of $Q_{EC}(^{192}$At$) - B_f(^{192}$Po$) = 2.08$ MeV is predicted within the FRDM/FRLDM model, giving a possibility of β-decay feeding to excited states well above the fission barrier in the daughter ^{192}Po. Even a larger Q_{EC}-B_f difference is expected if one uses the TF model. In agreement with these predictions, a large βDF probability, of the order of 7%–35%, depending on a number of assumptions, was deduced for ^{192}At in a SHIP experiment at GSI; see details in Ref. [11]. For ^{194}At, the calculated FRDM/FRLDM estimate is $Q_{EC}(^{194}$At$) - B_f(^{194}$Po$) = -0.04$ MeV, which is reflected in a much smaller measured $P_{\beta\mathrm{DF}}$ value of about 1% for this isotope [11]. We note that again a larger difference of

$Q_{EC}(^{194}$At$) - B_f(^{194}$Po$) = 1.71$ MeV is expected from the TF model.

For the βDF of ^{196}At, a value of $Q_{EC}(^{196}$At$) - B_f(^{196}$Po$) = -1.19$ MeV can be obtained based on the FRDM/FRLDM approach; thus, only a subbarrier fission of the daughter ^{196}Po should be expected in this model. Within the TF framework, the $Q_{EC}(^{196}$At$)$ and $B_f(^{196}$Po$)$ are nearly the same; thus, also only the subbarrier fission is expected within this model. Based on these reasons, a smaller $P_{\beta\mathrm{DF}}$ value is expected for ^{196}At in comparison with the lighter isotopes ^{192,194}At.

Prior to the present work at the On-Line Isotope Mass Separator (ISOLDE), almost all previous investigations produced ^{196}At in complete fusion reactions with heavy ions. This type of reaction resulted in the presence of other neighboring isotopes, originating from different xn, pxn, and αxn evaporation channels of these reactions.

First, identification of ^{196}At was performed by Treytl and Valli [18] using the complete fusion reactions ^{185}Re(^{20}Ne,xn)$^{205-x}$At and ^{187}Re(^{20}Ne,xn)$^{207-x}$At. Around 60×10^3 α counts of ^{196}At were detected. A single α decay with $E_\alpha = 7055(7)$ keV and a half-life of 0.3(1) s was observed (see Table I). Several other studies, shown in Table I, followed. We explicitly mention here only the recent study by Kalaninová *et al.* [19], which, based on the observation of several tens of events, reported two α-decay lines of ^{196}At with the energies of 7045(5) and 6732(8) keV, and a half-life of 350(90) ms was deduced for this isotope.

The first βDF study of ^{196}At was performed by Lazarev *et al.* [20]. The authors used a fusion evaporation reaction ^{159}Tb(^{40}Ca,$3n$)^{196}At and a rotating drum system surrounded by mica foil fission detectors. Owing to the use of an

unselective technique, the source of the recorded fission fragments could not be inferred directly. An apparent half-life for the fission fragments of $0.23^{+0.05}_{-0.03}$ s could be deduced, which was in agreement with the half-life of the assumed precursor nucleus ^{196}At, which was known at that time. Data from a number of irradiations with different projectile-target combinations further established the candidate precursor as ^{196}At.

II. EXPERIMENTAL SETUP

A. Production of the ^{196}At beam at RILIS + ISOLDE

To study ^{196}At in this work, two experiments were performed at the ISOLDE facility [21] at CERN. Experiment I utilized the High Resolution Separator (HRS) and Experiment II used the General Purpose Separator (GPS). In both experiments, the Resonance Ionization Laser Ion Source (RILIS) was used [22] in conjunction with mass separation, allowing samples of ^{196}At of higher purity to be obtained in comparison with the previous studies. Owing to much higher α-decay statistics in our experiments ($\sim 1.22 \times 10^6$ α decays in Experiment I for all ^{196}At peaks) and the use of high-purity germanium (HPGe) detectors, we were able to identify for the first time several α decays of ^{196}At to excited states in its daughter ^{192}Bi (the so-called fine-structure, f.s., α decays, Sec. III A) and to construct a more detailed α-decay scheme for this nucleus. New information on the low-energy excited states in the daughter isotope ^{192}Bi was also derived. The α decay and β-delayed fission of ^{196}At were also studied in detail in Experiment II at GPS ($\sim 6.22 \times 10^7$ α decays in the main ^{196}At peak), which is discussed in Sec. IV. Part of the βDF data resulting from this study was recently published by Ghys *et al.* [12].

Both experiments used the same experimental and analysis techniques, differing only in the use of HRS or GPS. ^{196}At nuclei were produced in spallation reactions by impinging an 1.8-μA (on average) proton beam of 1.4 GeV from the CERN Proton Synchrotron Booster on a thick 50 g/cm^2, UC$_x$ target of the HRS or GPS of ISOLDE. The proton beam structure consisted of a series of 30–40 2-μs proton pulses (depending on the runs), separated by a 1.2-s period and grouped together in a so-called "supercycle." After production in the target, the neutral reaction products diffused to a hot cavity ion source where the astatine isotopes were selectively ionized via a three-step ionization path to the 1^+ charge state using RILIS. The astatine ionization scheme was recently developed in dedicated experiments by Rothe *et al.* [23]. The selectively ionized ions were extracted from the ion source, accelerated to energies of 30 keV, and mass separated with the HRS or GPS.

B. Detection system

For the sake of consistency of the discussion, only a short description of the detection system is provided here; for further details, see Refs. [24–27]. The decays of ^{196}At and its daughter products were observed using the windmill (WM) detector system [24,27]. The mass-separated ions were implanted, through an 8-mm-diameter hole of an annular silicon detector (denoted further as Si1), into one of ten 20 μg/cm^2 thick

carbon foils [28] mounted on a rotating wheel, approximately 6 mm behind the Si1 (the so-called "implantation position" of the WM). The depleted layer of the annular detector has a thickness of 300 μm and a 450 mm^2 active area. A second circular detector (Si2) with a depletion depth of 300 μm and an active area of 300 mm^2 was situated $\sim$4 mm behind the foil. The two silicon detectors allowed measurements of twofold coincident fission fragments, along with α particles and single fission fragments. The detection efficiency for an α particle or single fission fragment in either of the detectors was $\sim$51%. For coincident fission fragments the detection efficiency was $\sim$16%. To detect conversion electrons, α particles, and fission fragments, the electronics of the detectors were set to record events with energy from $\sim$200 keV to 100 MeV. The necessity of such a broad energy range resulted in a worse energy resolution for the α particles, being in the range of $\sim$45–53 keV full width at half maximum (FWHM) in both runs.

The measurements were performed in cycles, whereby the implanted activity was first measured (also during implantation) at the "implantation position" for the duration of the supercycle. After the end of the supercycle, the irradiated foil was moved towards the so-called "decay position" situated at 144° relative to the implantation position, simultaneously introducing a new carbon foil at the irradiation position for the fresh implantation. A pair of silicon detectors, Si3 and Si4, were placed at the decay position, surrounding the carbon foil in close geometry from both sides. They were used to measure the remaining longer-lived daughter products. Both Si3 and Si4 had the same energy range as Si1 and Si2.

While no Ge detectors were used in the Experiment II at GPS, two HPGe detectors with relative efficiencies of 90% and 70% were exploited for a part ($\sim$30 min) of Experiment I at HRS. They were placed as close as possible behind and to the side of the windmill vacuum chamber and were efficiency and energy calibrated using the standard calibration sources of ^{152}Eu, ^{60}Co, and ^{133}Ba.

III. α DECAY OF ^{196}At: RESULTS AND DISCUSSION

A. α- and α-γ-decay spectra

As mentioned in the Introduction, approximately 50 times more α decays of ^{196}At were collected in Experiment II at GPS in comparison with the HRS experiment, but the quality of the data and extracted information is very different. Namely, as shown below, owing to the availability of HPGe detectors and the much cleaner spectra obtained during the HRS experiment, they were used in the first step of the data analysis for f.s. α-decay studies and for the deduction of α- and β-decay branching ratios for ^{196}At. In the subsequent step, the more abundant GPS data were used for βDF investigation.

Figures 2(a) and 2(b) show parts of the energy spectra measured in Si1 and Si2 for the GPS and HRS runs, respectively. As seen in Fig. 2(a), during the GPS experiment there was mass contamination from the heavier $^{197–201}$At isotopes (and some Rn isotopes), which is seen via the presence of their α decays. This is attributable to the lower GPS mass-resolving power and, possibly, a nonoptimal GPS tuning in the Experiment II. One can only see the "main" 7053-keV peak of ^{196}At
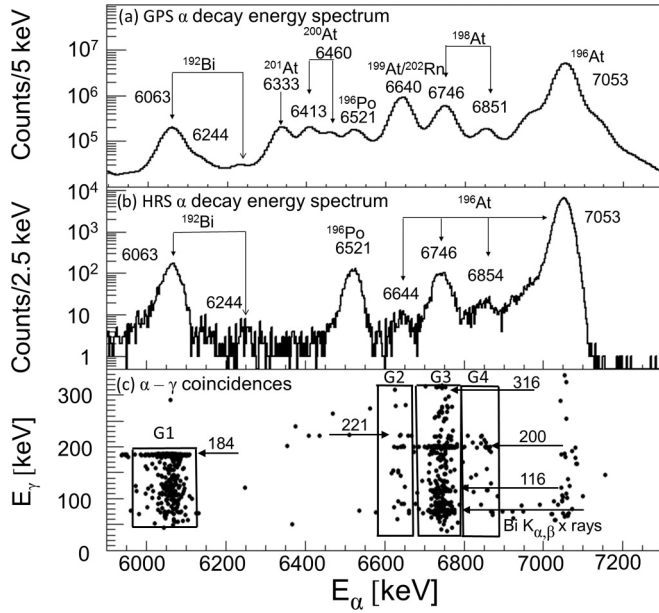
FIG. 2. (a) Part of the α-decay spectrum measured in the GPS experiment and summed from the Si1 and Si2 detectors. The peaks are marked with their energies (in keV) and the isotopes they belong to. (b) The same for the HRS experiment, but only part of the data collected during $\sim$30 min is shown, for which respective coincidence α-γ data are also available and shown in panel (c); see text. (c) The prompt α-γ coincidence plot for the α decays from (b), measured within the time interval of $\Delta T(\alpha - \gamma) \leqslant 600$ ns.

FIG. 3. Projections on the E_γ axis of the α-γ matrix, shown in Fig. 2(c), obtained by gating on (a) the region "G1," (b) the region "G2," (c) the region "G3," and (d) the region "G4." The γ-ray peaks are labeled by their energies in keV.

$(6.22 \times 10^7$ counts) with no f.s. α decays visible. In contrast to this, owing to the higher resolving power of HRS and the use of extra slits in the respective beam line of ISOLDE, these contaminants are fully absent in the experiment at HRS; see Fig. 2(b). As shown below, only α decays of ^{196}At, and of its daughter products, ^{192}Bi (after α decay) and ^{196}Po (after β decay), are present. Approximately $\sim$1.02 $\times 10^5$ counts are observed in the 7053-keV peak of ^{196}At in Fig. 2(b), which shows only a subset of 30 min of data collection when the HPGe detectors were connected. With full statistics the number of counts observed in the HRS experiment in the ^{196}At main peak is 1.19×10^6.

Seven α-decay peaks are seen in Fig. 2(b), including the known f.s. and main α decays of ^{196}At at the energies of 6746(5) keV (reported as 6732(8) keV in study [19]) and at 7053(5) keV (7045(5) keV in Ref. [19]), respectively. As shown below, the two previously unobserved α decays with the energies of 6644(8) and 6854(6) keV will be also attributed to f.s. decay of ^{196}At. Of the remaining three peaks, those at 6063(5) and 6244(10) keV are attributable to known α decay of ^{192}Bi [tabulated energies of 6060(5) and 6245(5) keV respectively], produced after α decay of ^{196}At, and the 6521(5)-keV peak is attributable to ^{196}Po [tabulated energy value of 6521(5) keV] produced by the β decay of ^{196}At.

Figure 2(c) shows prompt α-γ coincidences for α decays from panel (b), within a 600-ns coincidence time interval. The small number of events in the broad range of γ-ray
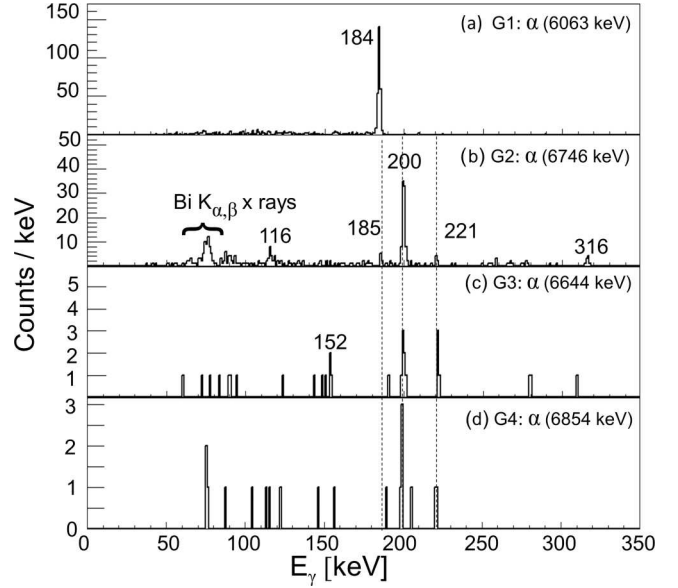
energies in coincidence with the main 7053-keV peak of ^{196}At is considered as random. Four areas of interest are marked by "G1"–"G4" in Fig. 2(c). The projections on the γ-energy axis from these four regions are shown in Figs. 3(a)–3(d).

Figures 2(c) and 3(a) show the known coincidences between the 6063(5)-keV α decay of ^{192}Bi and the 184-keV $E1$ γ-ray transition in the daughter ^{188}Tl [36]; see decay scheme in Fig. 4. As expected, no coincident events are seen for the full-energy 6244(10)-keV α decay of ^{192}Bi. By comparing the number of ^{192}Bi single α decays in Fig. 2(b) and coincident 6063-184-keV events in Fig. 3(a) the absolute γ-ray efficiency at 184 keV was deduced as 10(1)%. This value was used to normalize the γ-ray efficiency calibration curve produced with the use of the standard γ-ray sources.

A weak, but well-established group of α(6854 keV)-γ(199.9(1) keV) coincident events is seen in Fig. 2(c), and in the respective projection in Fig. 3(d). It has a total value $Q_{\alpha,\text{tot}} = Q_\alpha(6854) + E_\gamma(200) = 7196(6)$ keV, which is comparable, within the experimental uncertainty, to the value of $Q_\alpha = 7200(5)$ keV for the main 7053-keV α decay of ^{196}At; see Table I. On these grounds, the 6854-keV α decay was assigned as feeding to the previously unknown excited state at 200 keV above the low-spin state in ^{192}Bi, as shown in the decay scheme in Fig. 4.

Figure 3(b) shows the γ rays in coincidence with the 6746-keV f.s. α decay of ^{196}At. The energies of coincident γ rays are 115.7(3), 185.4(2), 199.9(1), 221.1(4), and 316.1(13) keV. We use the rounded energy values further in the text. The $Q_{\alpha,\text{tot}} = 7202(5)$ keV for the 6746-316-keV coincident events is in a good agreement with that for the 7053 keV decay (see Table I), which establishes an excited state at 316 keV in ^{192}Bi. We note that based on the observation of the 6732(8)-keV f.s. α decay of ^{196}At, the study by
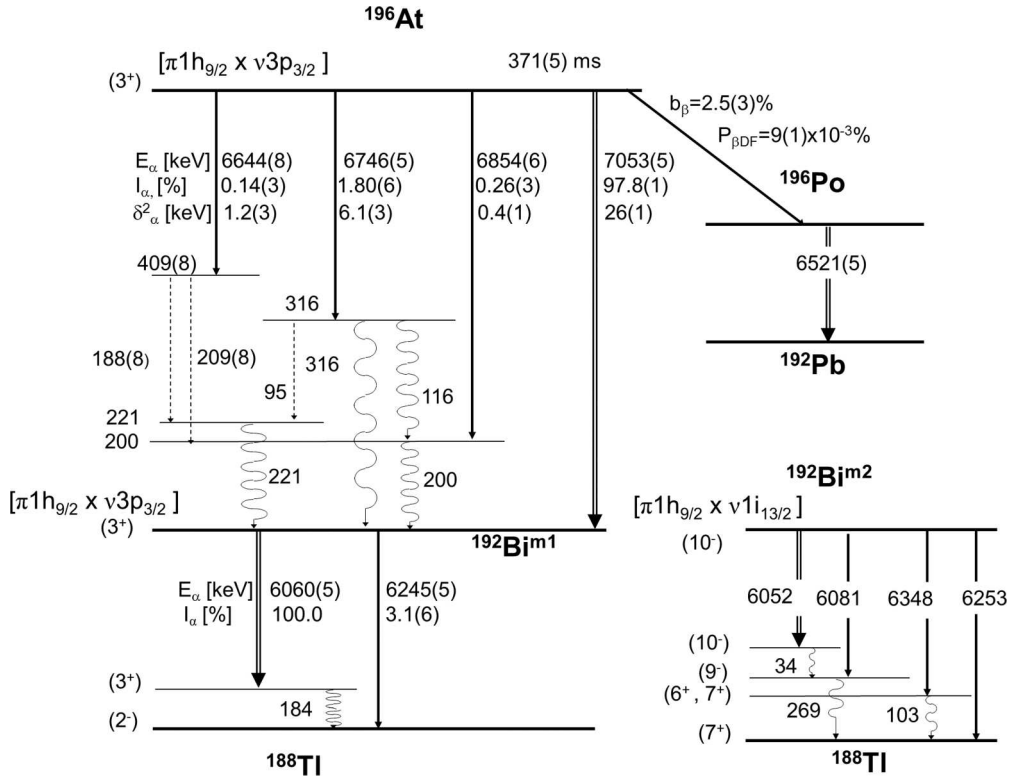
FIG. 4. Decay scheme of ^{196}At deduced in this work. The yet-unobserved 188(8)-, 209(8)-, and 95-keV γ decays are shown by dashed lines. For consistency of the discussion, the decay schemes of two isomeric states in the daughter isotope ^{192}Bi are also shown, including the tentative I^π values and configuration assignments taken from Ref. [36]. Owing to the yet-unknown relative excitation energy of the two α-decaying states in ^{192}Bi, we presently denote them as "m1" and "m2." The α-decay energies of 6060(5) and 6245(5) keV shown for ^{192}Bi^{m1} are also taken from Ref. [36] and are slightly different (within the experimental uncertainty) from the values of 6063(5) and 6244(10) keV measured in this work and shown in Fig. 2; see the main text.

Kalaninová *et al.* [19] proposed the existence of the 320(10)-keV excited state in ^{192}Bi. However, owing to low statistics, no respective γ rays were observed. The 6746-keV decay is also observed in coincidence with the 200- and 116-keV γ rays, whose energies sum up to exactly 316 keV. Therefore, we placed the 116- and 200-keV transitions in a cascade parallel to the 316-keV decay, with the 116-keV γ ray feeding the 200-keV state. It can be seen in Fig. 3(b) that the intensities of the 116- and 200-keV γ rays strongly differ, which is explained by the difference in their internal conversion, after the small difference in the respective detection efficiencies was accounted for; see further discussion and specific numbers of α-γ coincidences in Sec. III D.

The presence of a weak 6644(8)-keV α decay in Fig. 2(b) establishes a new excited state at 409(8) keV in ^{192}Bi, but no 6644-409(8)-keV α-γ coincidences were found in our analysis. However, as seen from Fig. 3(c), the 6644-keV decay is in coincidence with the 200- and 221-keV decays and tentatively with the weak 152.5(8)-keV γ decay. The presence of 6644-200- and 6644-221-keV coincidences requires the existence of 209(8)- and 188(8)-keV transitions, which are shown in Fig. 4 by dashed lines, as yet unobserved, probably owing to low statistics. Importantly, the 221-keV γ-ray decay is seen in coincidence with both the 6644- and the 6746-keV f.s. α decays. This fact suggests that an excited state at 221 keV should be present in ^{192}Bi, possibly deexciting

directly to the low-spin α-decaying state in this nucleus; see tentative placement of this level in Fig. 4. The observation of 6746-221 keV coincidences also requires the presence of (yet-unobserved) 95-keV decay from the 316-keV state to the 221-keV state. The weak 185-keV decay was not yet placed in the decay scheme of ^{196}At $\rightarrow$ ^{192}Bi. Table I shows the calculated experimental intensities for the α-decay peaks of ^{196}At, deduced from Fig. 2(b).

B. Half-life values of ^{196}At and ^{196}Po

The half-life of ^{196}At was determined using the HRS data only, as the GPS data contained strong contaminants, especially in the region of the fine-structure decays. The "grow-in and decay" method described in Ref. [25] was implemented for the independent half-life determination of the four α-decay transitions of ^{196}At. As an example, Fig. 5 shows the time distribution for the 7053-keV decay, following the implantation after two proton pulses separated by 1.2 s. Based on the fit as described in the figure, a half-life value of $T_{1/2}(^{196}$At$) = 371(5)$ ms was deduced, which is more precise than any of the previously deduced values; see Table I. Within a rather large experimental uncertainty, the half-life values for the three f.s. α decays are in agreement with each other and also with the half-life for the main 7053-keV decay; see Table I. Owing to the much lower intensities of the three
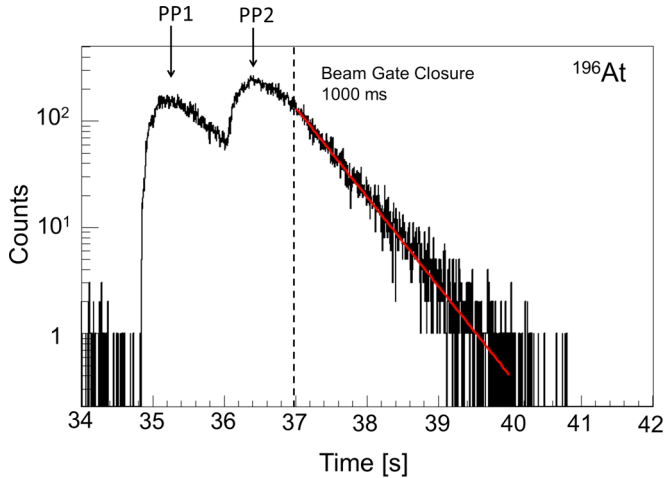
FIG. 5. The time distribution for the 7053-keV α decay of ^{196}At, following the implantation during two consecutive proton pulses PP1 and PP2, separated by 1.2 s. The decay part of the time distribution within the time interval of 37–41 s is fitted with an exponential function (shown in red), resulting in a value of $T_{1/2}(^{196}$At$) = 371(5)$ ms. The fit started 1000 ms after the PP2 proton beam impact, when the so-called ISOLDE "beam gate" was closed; thus, no new activity was deposited anymore on the carbon foil. The data from Si1 and Si2 are used.

FIG. 6. Half-life determination of ^{196}Po. The decay curve of the 6521-keV α decay of ^{196}Po in Si3 and Si4 at the decay position of the WM was fitted using an exponential (shown in red), resulting in a value of $T_{1/2}(^{196}$Po$) = 5.75(12)$ s. Note that the decay measurement stops at $\sim$42 s, which corresponds to the length of the proton synchrotron booster supercycle in this experiment, at which point the WM moves again by introducing the newly irradiated foil from the implantation position.

fine-structure decays, the half-life of the strongest 7053-keV ^{196}At peak was taken to be the overall half-life value of $T_{1/2}(^{196}$At$) = 371(5)$ ms.

The half-life of ^{196}Po (being the daughter of ^{196}At after β^+/EC decay) was also determined. As ^{196}Po is known to have a half-life of $\sim$6 s, the respective data from the 6521-keV α decay in Si3 and Si4 detectors at the decay position were utilized. As no beam implantation occurs at the site of Si3/Si4 and owing to the relatively short half-life of the parent ^{196}At, which totally decays either at the implantation position or during the $\sim$0.8-s rotation of the WM wheel, the Si3/Si4 detectors only measure the decay of daughter products which are left on the carbon foil. Therefore, an exponential function was fitted to the curve as seen in Fig. 6, whereby the half-life $T_{1/2}(^{196}$Po$) = 5.75(12)$ s was deduced. This value is in agreement with, but more precise than, the previous values of 5.5(5) s [37], 5.8(2) s [38], and 5.8(2) s [39].

C. α- and β-decay branching ratios of ^{196}At

Owing to the purity of the ^{196}At sample, the HRS data set was used to determine the β- and α-decay branching ratios, b_β and b_α, of this isotope. In particular, the b_α value was deduced by comparing the number of α decays of ^{196}At with the sum of all decays of this isotope, according to

$$b_\alpha(^{196}\text{At}) = \frac{N_\alpha(^{196}\text{At})}{N_\beta(^{196}\text{At}) + N_\alpha(^{196}\text{At})}, \tag{1}$$

where N_β and N_α are the number of β and α decays of ^{196}At, respectively. The $N_\beta(^{196}$At$)$ value cannot be measured directly in our experiment, but it is equal to the total number of the daughter ^{196}Po nuclei, which is deduced from the number of
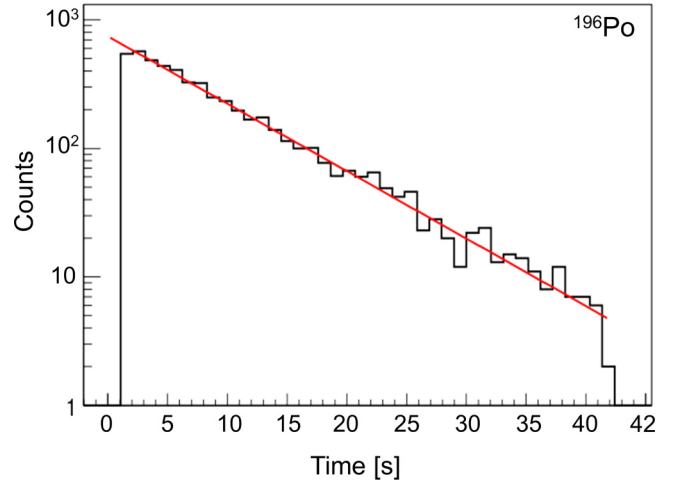
observed α decays of ^{196}Po, according to

$$N_\beta(^{196}\text{At}) = N(^{196}\text{Po}) = \frac{N_\alpha(^{196}\text{Po})}{b_\alpha(^{196}\text{Po})} \tag{2}$$

and by using the α-decay branching ratio $b_\alpha(^{196}$Po$) = 94(5)\%$ [39]. For the reader convenience, we refer to Fig. 2(b) with respect to how the respective numbers of $N_\alpha(^{196}$Po$)$ and $N_\alpha(^{196}$At$)$ were defined, while the full HRS data set was used for the determination of final values.

However, two corrections for the $N_\alpha(^{196}$Po$)$ number should be implemented. First, the number of ^{196}Po α decays had to be corrected for a possible small direct production of ^{196}Po in the target, rather than as a daughter product of ^{196}At. This was done by comparing the α-decay spectra measured with the lasers tuned on the ionization of astatine and with the resonant transition laser blocked. With the laser blocked, no astatine was present in the spectra, but a small number of α decays of ^{196}Po was evident, indicating its direct production in the target by a surface ionization in the ion source. The amount of directly produced ^{196}Po was estimated as $\sim$0.43% of the total ^{196}Po α decays measured in the HRS run and was subtracted from the total number of counts in the ^{196}Po peak.

The second correction accounts for the movement of the windmill's wheel at the end of each supercycle ($\sim$42 s). Owing to the relatively short half-life of ^{196}At, it fully decays at the implantation position, as the last implantation in the supercycle always happened at least 1.2 s before the WM's wheel movement. In contrast to this, owing to the 5.75-s half-life for ^{196}Po, part of its decay happened both during the 0.8-s WM's wheel movement and also at the decay position, where the α decays were measured by the Si3 and Si4 detectors. The respective correction accounted for 2.3% of the total number

of counts at the implantation and decay positions. As no recoil can escape the foil after β decay, no respective corrections were required.

After these corrections had been implemented, the experimental branching ratios of $b_\beta = 2.5(3)\%$ and $b_\alpha = 97.5(3)\%$ were deduced for the first time for ^{196}At.

The previously reported estimate of $b_\beta(^{196}$At$) \sim 4.9\%$ quoted in Ref. [40] was calculated from the QRPA β-decay theory [41]. Despite being approximately a factor of 2 larger than our experimental value, the previous estimate can be considered as being in reasonable agreement with our data, which also shows a quite good reliability of the model [41] for this case.

D. Multipolarity of the 200-, 116-, and 316-keV γ rays in ^{192}Bi

The γ-ray transitions that follow the f.s. α decay of ^{196}At are all prompt, which limits their multipolarity to $E1$, $M1$, or $E2$. Based on the estimation of the total conversion coefficients α_{total}, we can deduce more precise multipolarity for the 200-, 116-, and 316-keV decays.

We start from the generic expression

$$N_\alpha = \frac{N_{\alpha\gamma}}{\varepsilon_\gamma}(1 + \alpha_{\text{tot}}), \qquad (3)$$

where N_α is the number of α decays for a specific α line in the singles spectrum in Fig. 2(b), $N_{\alpha\gamma}$ is the respective number of α-γ coincidences observed in Fig. 2(c), ε_γ is the Ge detector efficiency at a specific energy, and α_{tot} is the total conversion coefficient of the respective γ ray.

As shown in Fig. 4, the 316-keV level, which is fed by the 6746-keV decay, deexcites by a cascade of coincident 200- and 116-keV transitions and also by a weak crossover 316-keV decay. Based on the above, one can write the intensity balance [see Eq. (4)] between the feeding 6746-keV α decay and the subsequent deexcitation by accounting for the coincident nature of 116- and 200-keV decays. The latter requires that their intensities be the same after the γ-ray efficiency and internal conversion corrections were implemented:

$$
\begin{aligned}
N_\alpha(6746) &= \frac{N_{\alpha(6746)\gamma(200)}}{\varepsilon_{\gamma(200)}}(1 + \alpha_{\text{tot}(200)}) \\
&\quad + \frac{N_{\alpha(6746)\gamma(316)}}{\varepsilon_{\gamma(316)}}(1 + \alpha_{\text{tot}(316)}) \\
&= \frac{N_{\alpha(6746)\gamma(116)}}{\varepsilon_{\gamma(116)}}(1 + \alpha_{\text{tot}(116)}) \\
&\quad + \frac{N_{\alpha(6746)\gamma(316)}}{\varepsilon_{\gamma(316)}}(1 + \alpha_{\text{tot}(316)}). \qquad (4)
\end{aligned}
$$

As part of the intensity balance according to Eq. (4), one also needs to reproduce the observed intensity of the Bi K x rays in Fig. 3(b), which puts yet another constraint on the possible multipolarities.

Therefore, to deduce the total conversion coefficients (thus, multipolarities) and the possible mixing ratios for the 116- and 200-keV γ rays, we used the number of $N_\alpha(6746) = 1783(43)$ counts from Fig. 2(b), corrected for the contribution of up to at most 8% (as shown below) owing to the 6746-316-keV decay branch. Based on the values of $N_{\alpha\gamma}(6746\text{-}200) = 88$ cts and $N_{\alpha\gamma}(6746\text{-}116) = 23$ cts taken from Fig. 3(b) and corrected for respective γ-ray efficiencies, the total experimental conversion coefficients of $\alpha_{\text{tot}}(116) = 5.1(5)$ and $\alpha_{\text{tot}}(200) = 0.9(1)$ were deduced. The comparison with the calculated total conversion coefficients from Ref. [42] $[\alpha_{\text{tot}}(116,M1) = 6.68$, $\alpha_{\text{tot}}(116,E2) = 3.61$, $\alpha_{\text{tot}}(200,M1) = 1.42$, $\alpha_{\text{tot}}(200,E2) = 0.45]$ suggests a mixed $M1 + E2$ character for both 116- and 200-keV γ rays, with the mixing ratios of 50(5)% for both of them. This, in turn, defines the most likely multipolarity of $E2$ for the crossover 316-keV transition, which also determines that its contribution to the balance in Eq. (4) does not exceed 8%. We also note that the use of the deduced conversion coefficients allows us to reproduce quite precisely the observed amount of Bi K x rays in Fig. 3(b), which can also be considered as a proof of the applied procedure.

Thus, the decay of the 316-keV excited state in ^{192}Bi proceeds via the competing 316-keV $E2$ and 116-keV mixed $M1 + E2$ γ-ray transitions. A theoretical ratio of $I(116)/I(316) = 100$ for the intensities of the 116- and 316-keV decays was deduced according to the Weisskopf half-life estimates from Firestone [43] by accounting for the 50% $M1 + E2$ mixed character of the 116-keV transition. As the 316-keV decay was assigned an $E2$ multipolarity, the apparent difference between the observed (after all corrections) intensity ratio of $I(116)/I(316) \sim 12$ and expected ratio of 100 could possibly be explained by the well-known collective enhancement of $E2$ transitions in this region of nuclei. However, this inference remains to be confirmed by further studies.

E. Discussion of α decay of ^{196}At

For the convenience of the discussion, Fig. 4 shows the simplified α-decay schemes of both long-lived states in the daughter ^{192}Bi isotope, taken from Ref. [36]. The tentative spin/parity and configuration assignment of both states in ^{192}Bi, shown in Fig. 4, are based on the α-decay systematics; see discussion in Ref. [36]. As shown by our data, the observation of the 6063-184-keV α-γ coincidences clearly confirms that only the presumed $I^\pi = (3^+)\alpha$-decaying state in ^{192}Bi, resulting from the $(\pi h_{9/2} \otimes \nu p_{3/2})$ configuration, is populated by the decay of the parent ^{196}At. Based on the unhindered nature of the main 7053-keV decay of ^{196}At $[\delta_\alpha^2 = 26(1)$ keV], the same spin of $I^\pi = (3^+)$ and configuration of $(\pi h_{9/2} \otimes \nu p_{3/2})$ should be assigned to the ground state of ^{196}At, which was also proposed by the earlier studies, e.g., [19]. The reduced α-decay widths shown in Fig. 4 were calculated within the Rasmussen approach [44] by assuming $\Delta L = 0\,\alpha$ decays. Tentatively, based on the deduced γ-ray multipolarities for the 116 ($M1 + E2$), 200 ($M1 + E2$), and 316 ($E2$) keV transitions, a spin/parity of 2^+–4^+ should be proposed for the 200-keV state, and a range of spins 1^+–5^+ for the state at 316 keV. The specific choice for the latter should, however, respect the deduced $M1 + E2$ multipolarity assignment for the 116-keV decay.

To shed more light on the possible spin and configuration assignments for the excited states in ^{192}Bi, we consider the

respective hindrance factors (HFs) for f.s. α decays feeding to these states. The HF values for the f.s. α decays quoted below were calculated as the ratio between their reduced α-decay widths and the reduced width of the 7053-keV α decay. The quite small reduced α-decay widths for the f.s. 6644- and 6854-keV α decays indicate their hindered nature, with the respective hindrance factors of $\sim$22(6) and $\sim$65(17) relative to the 7053-keV decay. Especially for the 6854-keV decay, its relatively large hindrance factor cannot be explained only by the presumed small angular momentum change of $\Delta L = 2$ between the (3^+) parent and $(2^+/4^+)$ daughter state at 200 keV and would additionally require a configuration change. However, the decay to the 316-keV state has a relatively small hindrance factor of 4.3(3) if one considers a $\Delta L = 0$ decay, which is close to the accepted definition of unhindered decays (HF < 4). If one considered a $\Delta L = 2$ decay (owing to deduced $E2$ multipolarity for the 316-keV transition), then even a smaller hindrance factor of HF = 2.6(3) would be obtained. In any case, the 6746-keV decay seems to lead to only a small configurational change between the parent and daughter states. However, with the presently available information on the hindrance factors and multipolarities of the 116-, 200-, and 316-keV transitions, no unambiguous information of the spin/parity for the 200-, 316-, and 221-keV states in ^{192}Bi can be deduced and we prefer to refrain from further speculations.

IV. β-DELAYED FISSION OF ^{196}At

A. Fission-fragment energy and mass spectra

The β-delayed fission of ^{196}At(fission of ^{196}Po after β^+/EC decay of ^{196}At) has been observed in the experiments at HRS and GPS, with 14 and 273 fission events found in the respective data sets. Therefore, in the following only GPS fission data are discussed. The energy spectrum of single fission events observed at GPS in either the Si1 or the Si2 detector in the energy range 30–90 MeV is shown in Fig. 7.
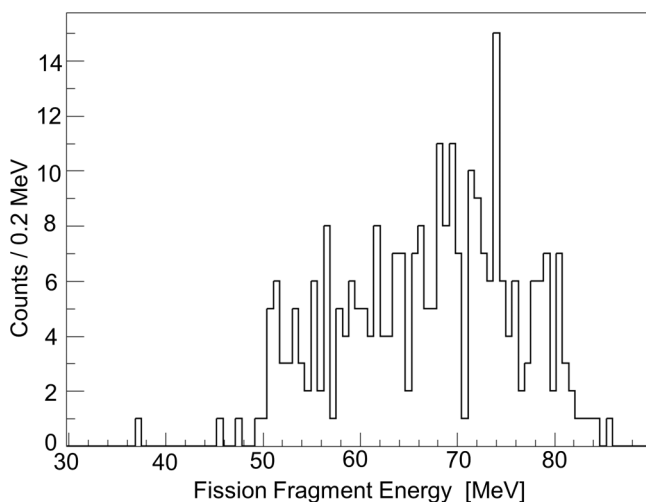
FIG. 7. Calibrated energy spectrum of single fission events in the β DF of ^{196}At, measured in the detectors Si1 and Si2 during the GPS run.
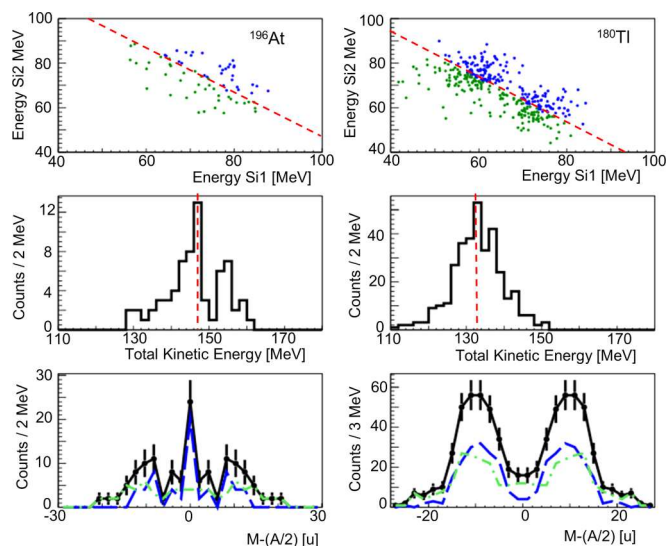
FIG. 8. Comparison of βDF data for ^{196}At (left column, present work) and for ^{180}Tl (right column, data from Ref. [26]). (Top row) The 2D energy distributions of coincident fission fragments in the two silicon detectors. (Middle row) The total kinetic-energy distributions. The red dashed line in the top two rows corresponds to respective most probable TKE values of ^{196}Po and ^{180}Hg; see text. (Bottom row) The FF mass distributions. The mass distributions shown by the black lines are for all observed events, while those shown by the dot-dashed green line and the dashed blue line correspond to events with the TKE values below and above the most probable TKE values, respectively.

Among the 273 registered fission fragments there were 68 coincident events, whereby one fission fragment was measured in Si1 and the other one in Si2. Only for these coincident events can fission-fragment masses be deduced from the measured fragment energies, following the well-accepted Schmitt calibration method introduced in Refs. [45,46]. This procedure accounts for the pulse-height defect of silicon detectors when heavy ions are being measured. The calibration procedure also involved measurements with separated fission fragments in an experiment at the Lohengrin spectrometer at ILL as described in Ref. [26]. This method was applied for our recent βDF measurements for ^{178,180}Tl, ^{194,196}At, and ^{202}Fr [12,26,47].

The resulting fission-fragment (FF) energy, total kinetic energy (TKE), and FF mass distribution spectra for βDF of ^{196}At are shown in the top, middle, and bottom panels of the left column of Fig. 8, respectively. For a comparison, the βDF data for ^{180}Tl from [12,26] is provided in the right column of the same figure.

For consistency of discussion, we briefly remind the reader of the main conclusions derived for the βDF of ^{180}Tl, for which approximately four times higher statistics were collected than for ^{196}At, including coincidence FF-γ-ray data. The two-dimensional Si1-Si2 coincidence plot for βDF of ^{180}Tl in Fig. 8 (top right panel) shows two distinct clusters of points, clearly demonstrating the asymmetric fission of the daughter (after β^+/EC decay) isotope ^{180}Hg. The respective TKE plot (middle right panel), showing a single Gaussian shape with the most probable value of TKE(^{180}Hg) = 133.2(14) MeV and

FWHM of 15.0(9) MeV [26], proves that only one fission mode is present in ^{180}Hg in this case. The total FF mass distribution (black line) in the bottom right panel for ^{180}Hg clearly shows an asymmetric distribution with the most probable heavy and light FF masses of $M_H = 100(1)$ and $M_L = 80(1)$. To summarize, all three plots clearly demonstrate that in the fission of ^{180}Hg (βDF of ^{180}Tl) only a single (asymmetric) fission mode is present.

A clear contrast can be seen between the βDF of ^{180}Tl and that of ^{196}At. Whereas ^{180}Tl data show two distinct clusters in the 2D coincidence plot, a broad FF area is observed for ^{196}At, as seen in the top left panel of Fig. 8. Furthermore, instead of a single Gaussian-like TKE distribution observed for ^{180}Hg, the TKE distribution for ^{196}Po is much broader, suggesting that fission does not occur via a single fission mode. Fitting this whole broader distribution with a single Gaussian fit gives the most probable value of TKE(^{196}Po) $= 147(1)$ MeV with FWHM of 24.2(9) MeV. For further reference, the points in the top row of Fig. 8 that have TKE values above and below the respective most probable TKE values are shown by blue and green, respectively.

The black solid line in the bottom left panel of Fig. 8 shows that ^{196}At has a triple-humped mass distribution, with the most probable FF masses, deduced from the Gaussian fit, being 88(2), 98(2), and 108(2). Considering this information along with the broader TKE distribution gives compelling evidence that at least two distinct fission modes are present in the fission of ^{196}Po. The FF masses of $M_L = 88$ and $M_H = 108$ represent the light and heavy peaks of the asymmetric mass distribution, respectively, while the $M_S = 98$ corresponds to the symmetric mass distribution.

The difference in fission modes of ^{196}Po can further be investigated by deriving the mass distributions for events with the TKE values above and below the most probable TKE. The distributions for ^{180}Hg and ^{196}Po are shown by the blue dotted lines and solid green lines lines in the bottom row of Fig. 8. Importantly, both higher-TKE and lower-TKE mass distributions have the same two-humped structure in case of ^{180}Hg, which again confirms that only a single asymmetric fission mode is present in this nuclide. In contrast to ^{180}Hg, the FF of ^{196}Po with the higher TKE values, shown in blue, demonstrates a dominant symmetric mass split. The mass distribution of events with the lower TKE values, shown in green, clearly have a "mixed" character, with different intensity ratios for symmetric and asymmetric modes. A small contribution of asymmetric mode to symmetric mass distribution (and vice versa) in the two distributions is most probably attributable to the imperfect selection procedure for fission events, based on the most probable TKE value.

We note that the above-quoted FF mass values for ^{196}Po have been deduced by assuming no neutrons were emitted in fission. The detailed analysis of the possible neutron emission for the case of βDF of ^{180}Hg, where $\sim$4 times higher statistics were collected, including the measurements of γ rays [26], showed that, at most, one neutron could be emitted in that case. Therefore, we expect that the emission of neutrons in the low-energy fission of ^{196}Po should play a similarly weak role.

It was not possible to experimentally measure the Z values of the fission fragments with the current setup. However, a

rough estimate of the most probable fission fragments can be made if one applies the concept of the same neutron-to-proton ratio $N/Z \sim 1.33$ in the fissioning parent ^{196}Po and in the final fission fragments. Within this framework, the most probable fission fragments in the asymmetric mode are lying in the vicinity of ^{88}Sr and ^{108}Pd, while the most probable fission fragments in the symmetric mass split should be in the vicinity of ^{98}Mo.

Recently, the potential energy surface (PES) for the fission of ^{196}Po was calculated by using the microscopic Hartree-Fock-Bogoliubov (HFB) theory with D1S Gogny interaction; see Fig. 2 of Ref. [48]. The PES shows a broad and flat plateau with numerous weakly pronounced valleys and ridges, not exceeding 1–2 MeV energy difference. As also discussed in Ref. [12], such a pattern in the PES for ^{196}Po, without well-defined shell corrections, should lead to several fission paths possibly giving rise to a mixture of symmetric and asymmetric mass distributions, which is in agreement with our experimental data. This work therefore extends the previous studies of the multimodal fission [49] phenomenon in the transactinides to the very neutron-deficient nuclei in the lead region.

B. βDF probability of ^{196}At

By definition, the probability of βDF can be calculated from

$$P_{\beta\mathrm{DF}} = \frac{N_{\beta\mathrm{DF}}(^{196}\mathrm{At})}{N_\beta(^{196}\mathrm{At})}, \tag{5}$$

where $N_{\beta\mathrm{DF}}$ is the number of observed fission events and $N_\beta(^{196}$At), defined in Eq. (2), is the total number of ^{196}At nuclei that decay by β decay, both properly corrected for the difference in the respective detection efficiency for fission and α decays. Only the GPS data are used for $N_{\beta\mathrm{DF}}$. However, owing to the presence of contaminants in the ^{196}Po region for the GPS data in Fig. 2, the $N_\alpha(^{196}$Po) value could not be directly estimated from GPS data. Therefore, a ratio of counts in the 7053-keV ^{196}At peak and in the 6521-keV ^{196}Po peak from the HRS run was first derived [see, e.g., Fig. 2(b)]. This ratio was then used to estimate the number of ^{196}Po α decays in the GPS run based on the measured number of α decays of ^{196}At in the same experiment.

Following the above procedure, a value of $P_{\beta\mathrm{DF}}(^{196}$At) $= 9(1) \times 10^{-5}$ was deduced, which is much lower than the experimental values for ^{192,194}At. As mentioned in the Introduction, this is indeed expected owing to larger (negative) Q_{EC}-B_f values for ^{196}At in comparison to the lighter astatine isotopes.

Presently, this is one of the most precisely determined $P_{\beta\mathrm{DF}}$ values and will be furthermore used within the framework described in our study [13] to estimate the fission-barrier height for the daughter ^{196}Po.

V. CONCLUSIONS

We investigated the α-decay fine-structure and βDF properties of the neutron-deficient isotope ^{196}At produced by using the laser ionization and mass-separation techniques at ISOLDE. By exploiting the purity of the ^{196}At sample from the HRS of ISOLDE and a sensitive detection system, which

also included HPGe detectors, significantly improved data were collected. In particular, several new excited states in the daughter ^{192}Bi were identified and multipolarities of γ rays from their decay were deduced, which could be helpful for further in-beam studies of this isotope. The systematics of the βDF in the astatine chain was extended to ^{196}At and includes now three βDF isotopes ^{192,194,196}At.

[1] K. Heyde and J. L. Wood, Shape coexistence in atomic nuclei, Rev. Mod. Phys. **83**, 1467 (2011).

[2] H. Kettunen, T. Enqvist, T. Grahn, P. Greenlees, P. Jones, R. Julin, S. Juutinen, A. Keenan, P. Kuusiniemi, M. Leino, A.-P. Leppänen, P. Nieminen, J. Pakarinen, P. Rahkila, and J. Uusitalo, Alpha-decay studies of the new isotopes ^{191}At and ^{193}At, Eur. Phys. J. A **17**, 537 (2003).

[3] H. Kettunen, T. Enqvist, M. Leino, K. Eskola, P. Greenlees, K. Helariutta, P. Jones, R. Julin, S. Juutinen, H. Kankaanpaa, H. Koivisto, P. Kuusiniemi, M. Muikku, P. Nieminen, P. Rahkila, and J. Uusitalo, Investigations into the alpha-decay of ^{195}At, Eur. Phys. J. A **16**, 457 (2003).

[4] A. N. Andreyev *et al.*, α-decay spectroscopy of the new isotope ^{192}At, Phys. Rev. C **73**, 024317 (2006).

[5] A. N. Andreyev *et al.*, α decay of ^{194}At, Phys. Rev. C **79**, 064320 (2009).

[6] U. Jakobsson *et al.*, Prompt and delayed spectroscopy of ^{199}At, Phys. Rev. C **82**, 044302 (2010).

[7] K. Auranen *et al.*, Spectroscopy of ^{201}At including the observation of a shears band and the $29/2^+$ isomeric state, Phys. Rev. C **91**, 024324 (2015).

[8] K. Andgren *et al.*, γ-ray spectroscopy of ^{197}At, Phys. Rev. C **78**, 044328 (2008).

[9] K. Auranen *et al.*, Experimental study of $\frac{1}{2}^+$ isomers in ^{199,201}At, Phys. Rev. C **90**, 024310 (2014).

[10] A. N. Andreyev, M. Huyse, and P. Van Duppen, Colloquium: Beta-delayed fission of atomic nuclei, Rev. Mod. Phys. **85**, 1541 (2013).

[11] A. N. Andreyev *et al.*, β-delayed fission of ^{192,194}At, Phys. Rev. C **87**, 014317 (2013).

[12] L. Ghys *et al.*, Evolution of fission-fragment mass distributions in the neutron-deficient lead region, Phys. Rev. C **90**, 041301 (2014).

[13] M. Veselský, A. N. Andreyev, S. Antalic, M. Huyse, P. Möller, K. Nishio, A. J. Sierk, P. Van Duppen, and M. Venhart, Fission-barrier heights of neutron-deficient mercury nuclei, Phys. Rev. C **86**, 024308 (2012).

[14] P. Möller, J. R. Nix, W. D. Myers, and W. J. Swiatecki, Nuclear ground-state masses and deformations, At. Data Nucl. Data Tables **59**, 185 (1995).

[15] P. Möller, A. J. Sierk, T. Ichikawa, A. Iwamoto, and M. Mumpower, Fission barriers at the end of the chart of the nuclides, Phys. Rev. C **91**, 024310 (2015).

[16] W. D. Myers and W. J. Świątecki, Thomas-Fermi fission barriers, Phys. Rev. C **60**, 014606 (1999).

[17] M. Wang, G. Audi, A. Wapstra, F. Kondev, M. MacCormick, X. Xu, and B. Pfeiffer, The Ame2012 atomic mass evaluation, Chin. Phys. C **36**, 1603 (2012).

[18] W. Treytl and K. Valli, Alpha decay of neutron deficient astatine isotopes, Nucl. Phys. A **97**, 405 (1967).

[19] Z. Kalaninová, S. Antalic, A. N. Andreyev, F. P. Heßberger, D. Ackermann, B. Andel, L. Bianco, S. Hofmann, M. Huyse, B. Kindler, B. Lommel, R. Mann, R. D. Page, P. J. Sapple, J. Thomson, P. Van Duppen, and M. Venhart, Decay of $^{201-203}$Ra and $^{200-202}$Fr, Phys. Rev. C **89**, 054312 (2014).

[20] Y. A. Lazarev, Y. T. Oganessian, I. V. Shirokovsky, S. P. Tretyakova, V. K. Utyonkov, and G. V. Buklanov, Inst. Phys. Conf. Ser. **132**, 739 (1992).

[21] E. Kugler, The ISOLDE facility, Hyperfine Interact. **129**, 23 (2000).

[22] V. N. Fedosseev, L. E. Berg, D. V. Fedorov, D. Fink, L. O. J., R. Losito, B. A. Marsh, R. E. Rossel, S. Rothe, M. D. Seliverstov, A. M. Sjodin, and K. D. A. Wendt, Upgrade of the resonance ionization laser ion source at ISOLDE on-line isotope separation facility: New lasers and new ion beams, Rev. Sci. Instrum. **83**, 02A903 (2012).

[23] S. Rothe *et al.*, Measurement of the first ionization potential of astatine by laser ionization spectroscopy, Nat Commun. **4**, 1835 (2013).

[24] A. N. Andreyev *et al.*, New Type of Asymmetric Fission in Proton-Rich Nuclei, Phys. Rev. Lett. **105**, 252502 (2010).

[25] J. Elseviers *et al.*, Shape coexistence in ^{180}Hg studied through the β decay of ^{180}Tl, Phys. Rev. C **84**, 034307 (2011).

[26] J. Elseviers *et al.*, β-delayed fission of ^{180}Tl, Phys. Rev. C **88**, 044321 (2013).

[27] M. D. Seliverstov *et al.*, Electromagnetic moments of odd-a $^{193-203,211}$Po isotopes, Phys. Rev. C **89**, 034323 (2014).

[28] B. Lommel, W. Hartmann, B. Kindler, J. Klemm, and J. Steiner, Preparation of self-supporting carbon thin films, Nucl. Instrum. Methods Phys. Res., Sect. A **480**, 199 (2002).

[29] K. Morita *et al.*, New α-decaying neutron deficient isotopes ^{197}Rn and ^{200}Fr, Z. Phys. A **352**, 7 (1995).

[30] T. Enqvist, K. Eskola, A. Jokinen, M. Leino, W. Trzaska, J. Uusitalo, V. Ninov, and P. Armbruster, Alpha decay properties of $^{200-202}$Fr, Z. Phys. A **354**, 1 (1996).

[31] Y. Pu, K. Morita, M. Hies, K. Lee, A. Yoshida, T. Nomura, Y. Tagaya, T. Motobayashi, M. Kurokawa, H. Minemura, T. Uchibori, T. Ariga, K. Sueki, and S. Shin, New α-decaying neutron-deficient isotope ^{196}Rn, Z. Phys. A **357**, 1 (1997).

[32] M. B. Smith *et al.*, Isomeric state in the doubly odd ^{196}At nucleus, J. Phys. G: Nucl. Part. Phys. **26**, 787 (2000).

[33] H. De Witte, A. Andreyev, S. Dean, S. Franchoo, M. Huyse, O. Ivanov, U. Köster, W. Kurcewicz, J. Kurpeta, A. Plochocki, K. Van de Vel, J. Van de Walle, and P. Van Duppen, Alpha-decay of neutron-deficient ^{200}Fr and heavier neighbours, Eur. Phys. J. A **23**, 243 (2005).

[34] M. Nyman, S. Juutinen, I. Darby, S. Eeckhaudt, T. Grahn, P. T. Greenlees, U. Jakobsson, P. Jones, R. Julin, S. Ketelhut, H. Kettunen, M. Leino, P. Nieminen, P. Peura, P. Rahkila, J. Sarén, C. Scholey, J. Sorri, J. Uusitalo, and T. Enqvist, γ-ray and decay spectroscopy of ^{194,195,196}At, Phys. Rev. C **88**, 054320 (2013).

[35] J. Uusitalo, J. Sarén, S. Juutinen, M. Leino, S. Eeckhaudt, T. Grahn, P. T. Greenlees, U. Jakobsson, P. Jones, R. Julin, S. Ketelhut, A.-P. Leppänen, M. Nyman, J. Pakarinen, P. Rahkila, C. Scholey, A. Semchenkov, J. Sorri, A. Steer, and M. Venhart, α-decay studies of the francium isotopes ^{198}Fr and ^{199}Fr, Phys. Rev. C **87**, 064304 (2013).

[36] P. Van Duppen, P. Decrock, P. Dendooven, M. Huyse, G. Reusen, and J. Wauters, Intruder states in odd-odd Tl nuclei populated in the α decay of odd-odd Bi isotopes, Nucl. Phys. A **529**, 268 (1991).

[37] A. Siivola, $^{193-200}$Po isotopes produced through heavy ion bombardments, Nucl. Phys. A **101**, 129 (1967).

[38] P. Van Duppen, E. Coenen, K. Deneffe, M. Huyse, and J. Wood, Low-lying $J^{\Pi} = 0^{+}$ states in ^{190,192}Pb populated in the α-decay of ^{194,196}Po, Phys. Lett. B **154**, 354 (1985).

[39] J. Wauters, P. Dendooven, M. Huyse, G. Reusen, P. Van Duppen, and P. Lievens, α-decay properties of neutron-deficient polonium and radon nuclei, Phys. Rev. C **47**, 1447 (1993).

[40] ENSDF, Evaluated Nuclear Structure Data File, http://www.nndc.bnl.gov/ensdf/ (2013).

[41] P. Möller, J. Nix, and K. Kratz, Nuclear properties for astrophysical and radioactive-ion-beam applications, At. Data Nucl. Data Tables **66**, 131 (1997).

[42] T. Kibédi, T. Burrows, M. Trzhaskovskaya, P. Davidson, and C. N. Jr., Evaluation of theoretical conversion coefficients using BrIcc, Nucl. Instrum. Methods Phys. Res., Sect. A **589**, 202 (2008).

[43] R. B. Firestone *et al.*, *Table of Isotopes*, 8th ed. (Wiley & Sons, New York, 1998).

[44] J. O. Rasmussen, Alpha-Decay Barrier Penetrabilities with an Exponential Nuclear Potential: Even-Even Nuclei, Phys. Rev. **113**, 1593 (1959).

[45] H. W. Schmitt, W. E. Kiker, and C. W. Williams, Precision Measurements of Correlated Energies and Velocities of ^{252}Cf Fission Fragments, Phys. Rev. **137**, B837 (1965).

[46] E. Weissenberger, P. Geltenbort, A. Oed, F. Gönnenwein, and H. Faust, Energy calibration of surface barrier detectors for fission fragments, Nucl. Instrum. Methods A **248**, 506 (1986).

[47] V. Liberati *et al.*, β-delayed fission and α decay of ^{178}Tl, Phys. Rev. C **88**, 044322 (2013).

[48] J. D. McDonnell, W. Nazarewicz, J. A. Sheikh, A. Staszczak, and M. Warda, Excitation-energy dependence of fission in the mercury region, Phys. Rev. C **90**, 021302 (2014).

[49] Y. Nagame and H. Nakahara, Two-mode fission - experimental verification and characterization of two fission-modes, Radiochim. Acta **100**, 605 (2012).